River Flow 2010 - Dittrich, Koll, Aberle & Geisenhainer (eds) - © 2010 Bundesanstalt für Wasserbau ISBN 978-3-939230-00-7

Flow Visualization of Mean and Coherent Flow Structures around T-type and L-type Groynes

A. Kadota & K. Suzuki
Department of Civil & Environmental Engineering, Faculty of Engineering, Ehime University, Matsuyama Ehime, Japan

E. Kojima
Graduate School of Science and Engineering, Ehime University, Matsuyama, Ehime, Japan

ABSTRACT: There are several types of groyne, such as T-type and L-type groynes, that have been constructed worldwide in accordance with different river environments. However, little information has been obtained on the structures of local flow and the development of large-scale vortices around differently shaped groynes. Because these flow structures are expected to significantly affect the formation of sand waves further downstream, this phenomenon should be considered systematically and in detail. To reveal such flow effects, flow is visualized around several types of groyne under emerged and submerged conditions in the present study by means of particle tracking velocimetry, which was developed especially for estimating velocity more accurately under conditions of large-velocity difference. To discuss the flow pattern around the groynes, statistical analysis is applied to estimate mean properties such as the Reynolds stress. In addition, conditional sampling analysis and the Weiss function are applied to reveal the coherent structures. The results show high-turbulence areas near the tips of groynes and strong vortex development downstream. The differences in flows around several types of groyne are the distributions of large areas of turbulence downstream.

Keywords: T-type and L-type groynes, Submergence effect, Conditional sampling analysis, Weiss function

1 INTRODUCTION

Several types of groyne have been used for the stabilization of banks, creating a navigation channel by confining the cross-sectional area and improving the habitat of flora and fauna, especially for large rivers worldwide.

The most important phenomena are local flow and local scour around the groyne tip. Therefore, turbulent flows around groynes have been studied experimentally and numerically in recent decades. Furthermore, there have been various studies on pollutant and sediment transport and related erosion (or scouring) around groynes in rivers and coastal regions.

The number of studies on flow patterns and transport processes around groyne-like structures increased with improved experimental and computational techniques. Chen & Ikeda (1997), Uijttewaal et al. (2001), and Weitbrecht & Jirka (2001) studied the flow patterns of gyres and mixing layers with respect to the aspect ratio (length of and distance between groynes). The exchange process between a main stream and an embayment was studied by Altai & Chu (1997), Uijttewaal et al. (2001), and Weitbrecht & Jirka (2001), who performed experimental studies using dye concentration analysis. In addition to the above studies, scouring processes were studied earlier by Garde et al. (1961), Gill (1972), and Kuhnle et al. (2002), who considered flow dynamics around the groyne tip.

The former studies focused mainly on local flow and local scour phenomena around straight (I-type) groynes. There are several types of groyne, such as T-type and L-type groynes, and these have been constructed worldwide in accordance with different river environments. However, little information has been obtained on detailed flow structures and bed variations around differently shaped groynes. Because high shear forces caused by coherent vortices in the mixing layer between the main stream and dead zone behind groynes largely affect the formation of sand waves further downstream, these flow phenomena should be considered systematically and in detail.

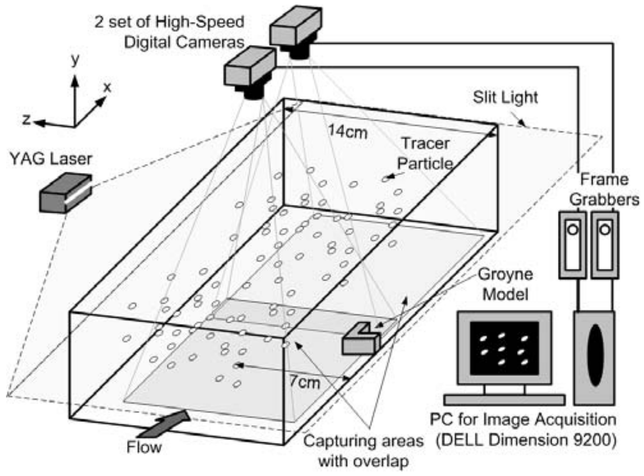

Figure 1. Experimental setup

The present study focuses on the effects of groyne shape on largely distributed and coherent and mean flow-structures in horizontal plane at downstream I-type, T-type, and L-type groynes. These flow structures are expected to affect the coherent vortices described the above. Experiments were conducted with models of the three types of groyne, and flow visualization and particle tracking velocimetry (PTV) were employed to analyze the resulting images. This method is preferred because of the large dynamic velocity range in the horizontal plane between the outside and inside of the dead zone behind the groyne. A two-dimensional PTV code programmed by Kadota et al. (2007) was used in this study. In this code, the advantages of the fast Fourier transform (FFT), combined with direct correlation methods, are used to speed up the calculation process because of the large number of large-sized images.

The experimental setup and analytical procedure are presented and the detailed flow structures around the different types of groynes in emerged and submerged conditions are discussed. Experimental results show that the distribution of large, shear-layer, coherent vortices changes greatly with the groyne type, and the turbulence effect for the L-type groyne is much smaller than that for the I-type groyne. These results will be applicable to the design of groynes for several purposes.

2 EXPERIMENTAL SETUP AND IMAGE ACQUISITION PROCESS

Experiments were conducted by means of flow visualization. The experimental flume is made of transparent acrylic materials and is 14 cm in width and 300 cm in length, as shown in Figure 1. In the flume, water flow is provided by a smoothly adjustable pump (maximum discharge $Q_{\max}$ = 3000 cm^3/s) that is controlled by a frequency converter (Toshiba VF-S9). The groyne model is also made of transparent acrylic plate to obtain enough slit light behind the groyne model. The groyne models are arranged beside the channel wall, as shown in Figure 1. The sizes and shapes of the scale models are shown in Figure 2. The scales are determined from the sizes of groyne length and river width in existing small Japanese rivers. The thickness of the transparent acrylic plate is 0.5 cm for all models. There are two L-type groyne models. One runs upstream (LU-type) and the other downstream (LD-type). Stream-wise lengths (L_f) are 2.5 cm for the L-type and T-type groyne models. Span-wise lengths (L_g) and the heights (H_g) of the models are 2.5 and 4.0 cm respectively in all cases. Flow discharge is defined as Q = 1000 cm^3/s in all cases and flow depths are 3.9 and 4.5 cm for emerged and submerged conditions respectively. The resulting Re number is about 7140.

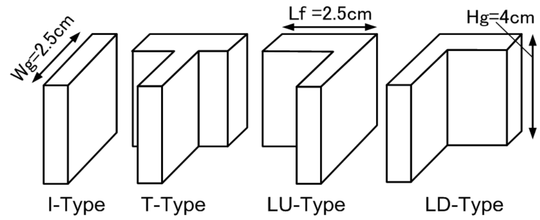

Figure 2. Types and scales of groyne model

It is necessary to conduct recording large-scale investigation with high accuracy because large vortices generated downstream are related to the separated flow at the tip of the groyne as described above. Therefore, in this flow visualization, two sets of digital cameras (ImperX VGA120) and closed circuit television lenses (Pentax C1614-M) are used. For illumination of tracer particles, a YAG laser light sheet (Katoko-ken, PIV Laser G50, 50 mW) is used with a light slit 0.5 mm wide. The height of the slit is set close to the surface of the groyne model. Images are recorded using frame grabber (Epix PIXCI-CL1) and image acquisition software (Epix XCAP-Ltd). The image size for one camera is 520 × 480 pixels in stream-wise and lateral directions respectively. The frequency of the recording is 109 Hz and one recording section with two cameras has an area of 17.65 cm by 8.17 cm with some overlap. For the tracer particle and its supply, ion-exchange resin (Diaion, Mitsubishi Chemical Co., diameter of 250–600 μm, density of 1.02 g/cm^3) with methyl alcohol is applied and seeded in the flowing water ensuring a homogeneous distribution. Two thousand images are recorded for all measurements using the above-mentioned recording system and processed as follows.

3 IMAGE PROCESSING AND ANALYSIS OF TUBULENCE STATISTICS

In the present study, the PTV method, which was coded for flow with a large velocity difference by Kadota et al. (2006), is adopted and implemented to calculate velocities quickly and accurately. This

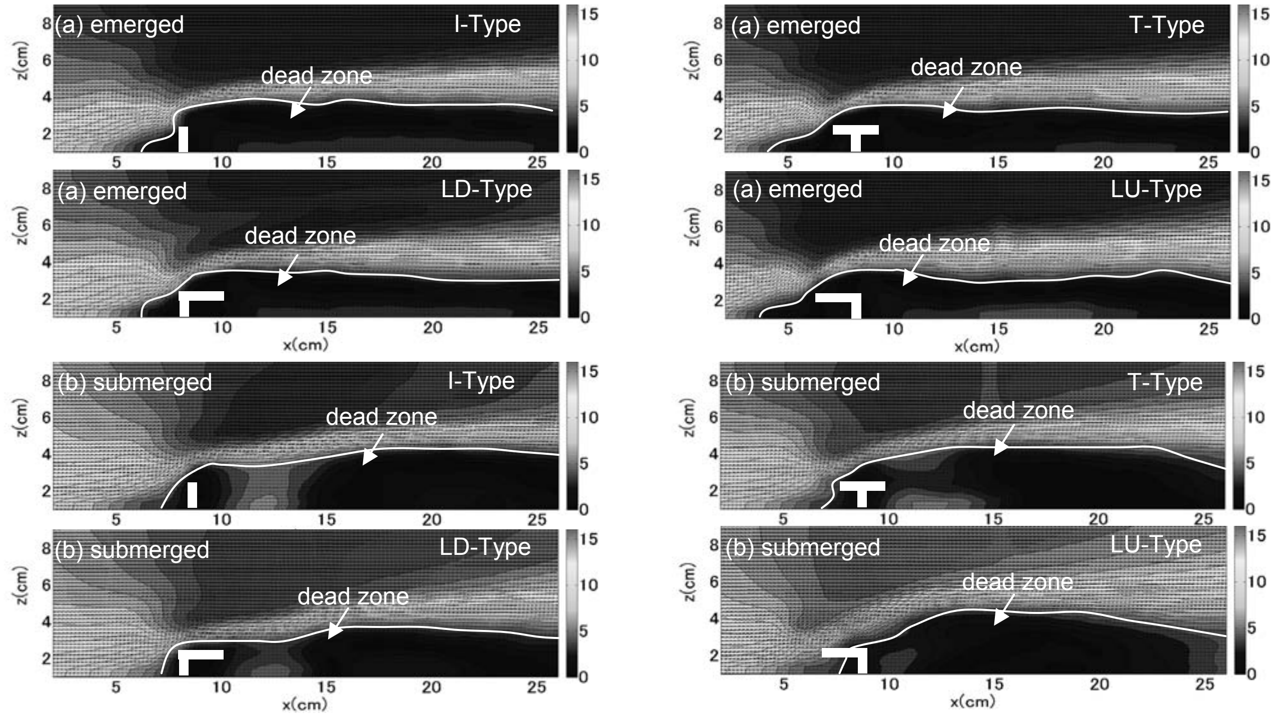

Figure 3. Magnitude of the mean velocity field around several types of groynes under emerged and submerged conditions

PTV code was programmed with consideration of speeding up calculations using the advantages of the FFT and direct correlation methods. The first temporal velocity is estimated by FFT cross-correlation and then the search area of direct correlation is determined around the first estimated vector point to estimate the more accurate second velocity. This reduces the useless search area and results in a procedure for fast correlation calculation. Before applying this code, some image pre-processing is done, such as subtracting the background, removing noise, binarization, and labeling of particle images.

In addition, interpolated vectors on a regular grid are applied for statistical analysis of the turbulence, as described below, because there is no deficit of vector points and a series of instantaneous vector profiles have to be used.

To reveal the coherent structures around the several types of groyne, conditional sampling analysis is applied to determine the advection of a coherent fluctuation pattern. The conditional averaging of an arbitrary sampling signal $\langle q(x,z,\Delta x,\Delta z,t,\tau)\rangle$ is defined as

$$\langle q(x,z,\Delta x,\Delta z,t,\tau)\rangle = \frac{\int_T q(x+\Delta x, z+\Delta z, t, \tau)\cdot I(x,z,t)\,dt}{\int_T I(x,z,t)\,dt} \tag{1}$$

where q represents the magnitude of the velocity fluctuations and the fluctuations (u, w) are determined from stream- and span-wise instantaneous velocities. x and z are the coordinates of the fixed point in the stream- and span-wise directions respectively. The fixed point is defined as near the tip of the groyne. Δx and Δz are distances from the fixed point. t and τ are the fixed and delay times respectively. $I(x, z, t)$ is the detection function for target coherent flow structures. The procedure for determining the detection function is described below and the results discussed.

In addition to the conditional sampling analysis, the Weiss function (Q-value) is applied for the instantaneous flow field. The function is defined as the difference between the squared shear (S) and squared vorticity (ω):

$$Q = S^2 - \omega^2$$

$$= \left(\frac{\partial u}{\partial x} - \frac{\partial w}{\partial z}\right)^2 + \left(\frac{\partial w}{\partial x} + \frac{\partial u}{\partial z}\right)^2 - \left(\frac{\partial w}{\partial x} - \frac{\partial u}{\partial z}\right)^2 \tag{2}$$

The first and second terms refer to the shear forces and the third term refers to the rotation force. Negative and positive Q-values indicate the dominance of rotation and shear forces respectively. The observation of an instantaneous Q-value-distribution can be regarded as the coherent structure of the shear and rotational motions.

4 RESULTS AND DISCUSSIONS

The turbulence flow structures around T-type and L-type groynes are compared with those around I-type groynes.

4.1 *Profiles of Mean Velocity and Reynolds Stress*

Figure 3 shows the mean vector profiles for I-type, T-type, and the two L-type groyne models under emerged and submerged conditions. These plane profiles are at 4.0 cm height above the

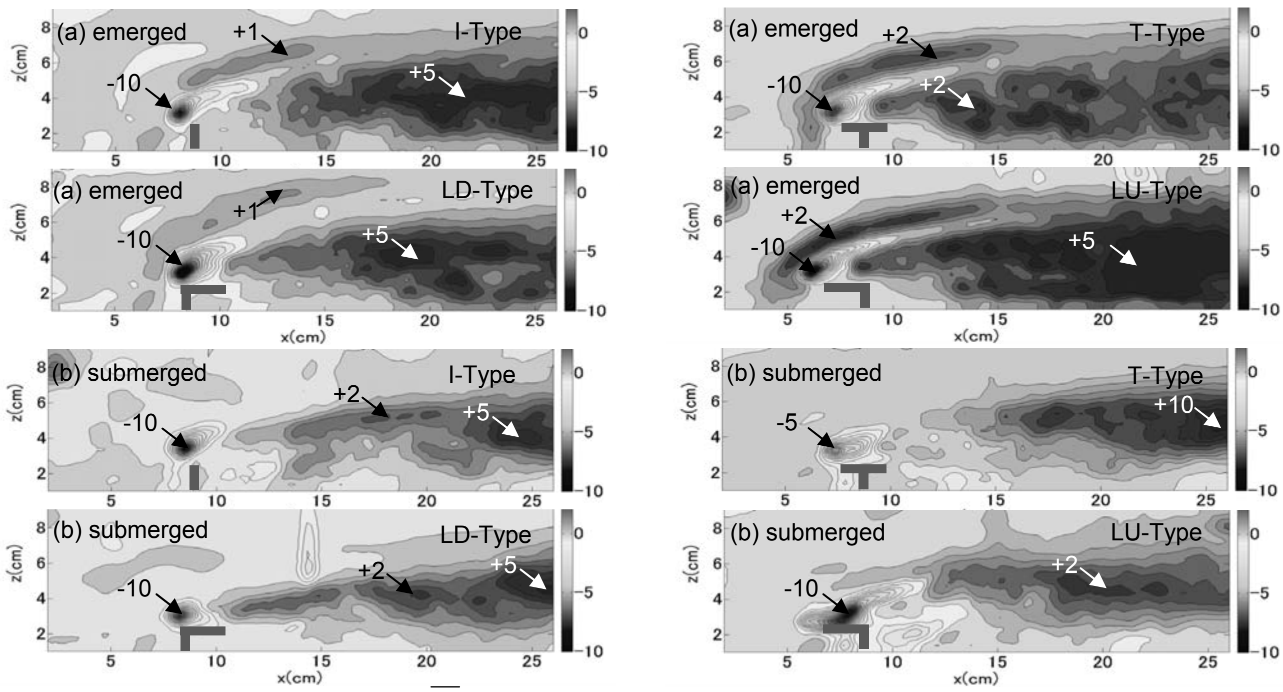

Figure 4. Reynolds stress distribution ($-\overline{uw}$) [cm/s] under emerged and submerged conditions

channel bed (near the top surface of the groyne model) and vectors are thinned to see clearly the contour map, which indicates the magnitudes of the vectors.

The difference between the profiles is seen in the areas downstream and upstream of the groyne tip. Especially for T-type and L-type groynes running upstream (LU-type), the dead zone is enlarged behind the groyne for submerged conditions compared with emerged conditions. On the other hand, the dead zone on the upstream side of the groyne is reduced. It is considered that the submerged flow on the surface of the groyne decelerates the flow near the groyne and thus produces a small difference of velocity. Under emerged conditions for these cases, flow from the upstream end is entrained into the upstream dead zone of the groyne. Therefore, the downstream dead zone is reduced. These tendencies are similar to experimental results from shallow flow visualization of an inclined groyne model (Weitbrecht 2004). In the case of the groyne running downstream (LD-type), there is less difference in the dead zone between emerged and submerged conditions.

In the vicinity of the groyne tip, a different velocity profile is seen around the LU-type groyne under submerged conditions. The velocity difference between the main stream and dead zone is significantly less. It is supposed that shear stress in the vicinity of the groyne tip is weakened, and thus, the effects on the transport phenomena of sediment and pollutant are small. The profile of the L-type groyne running downstream (LD-type) is similar to that of the I-type groyne, whereas the profile of the T-type groyne is similar to that of the LU-type. It is considered that these velocity profile areas are affected by the protuberance of the groyne. In terms of stabilizing the flow and bed conditions, the LU-type groyne is more suitable.

The above-mentioned typical patterns are also seen for profiles of the Reynolds stress in the cross-wise direction. Figure 4 shows the profiles of the Reynolds stress ($-\overline{uw}$) for emerged and submerged conditions. The Reynolds stress is largely related to shear stress, which affects transport phenomena such as those of sediment and pollutant materials, and is an important parameter for considering coherent flow structures.

In the cases of I-type and LD-type groynes, there is large negative stress distributed near the edge of the groyne under both emerged and submerged conditions. However, a different distribution is seen for T-type and L-type groynes. The large negative stress shifts downstream under the submerged condition, especially for the LU-type groyne, and it is distributed on the side surface of the groyne. This tendency is related to the dead zone and velocity difference area around the LU-type groyne as shown in the mean velocity profiles in Figure 3. The velocity difference area also shifts downstream.

Downstream of the groyne, there is large Reynolds stress distributed from the tip of the groyne caused by the velocity difference between the dead zone and main stream. In the cases of the groynes running upstream (T-type and LU-type), there is a significant large positive Reynolds stress. It is considered that a large-scale vortex structure will be generated in the downstream area.

Figure 5 shows the profiles of mean vorticity (ω). Clockwise (negative) circulating patterns are

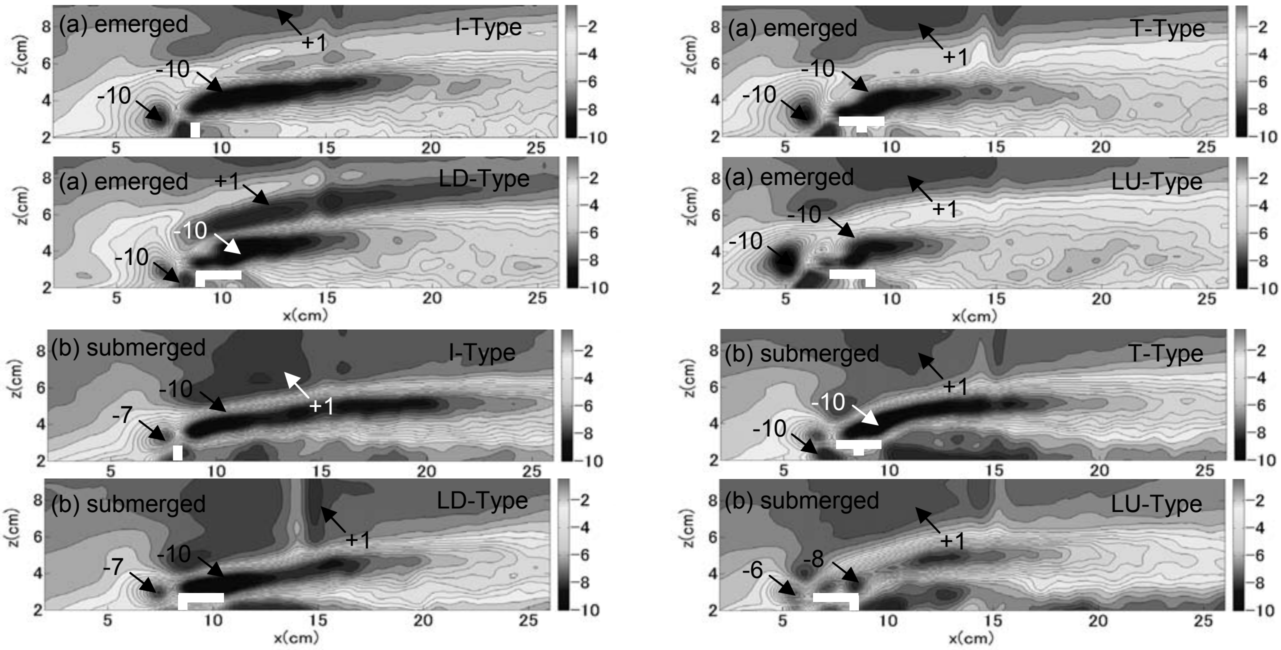

Figure 5. Mean vorticity distribution (ω) [cm/s] under emerged and submerged conditions

seen in both upstream and downstream areas around the groynes because the flow from upstream is entrained into dead zones.

In the case of a groyne running upstream (LU-type) under emerged conditions, there is a significant clockwise motion concentrated in the vicinity of the groyne tip because of the large velocity difference. Under submerged conditions, the clockwise motion grows downstream for the groyne running downstream (LD-type). Comparing with the mean velocity profile in Figure 3, the area of clockwise motion corresponds to the dead zone around the groyne. In the case where the dead zone on the upstream side of the groyne is smaller (I-type and LD-type), the clockwise motion tends to expand stream-wise.

In this section, the Reynolds stress and vorticity were mainly discussed in terms of mean flow structure. In the following section, the instantaneous coherent-flow structures are discussed by means of conditional sampling analysis and the Weiss function as instantaneous flow structures.

4.2 *Advection of instantaneous coherent flow pattern*

Figure 6 shows profiles and time variations of the Weiss function (Q-value) estimated from Equation (2) as instantaneous coherent flow patterns. In this figure, a white area indicates the dominance of shear force with a Q-value over +30 ($1/s^2$), and a gray area indicates the dominance of rotation with a Q-value less than –30 ($1/s^2$).

In all cases of emerged conditions in Figure

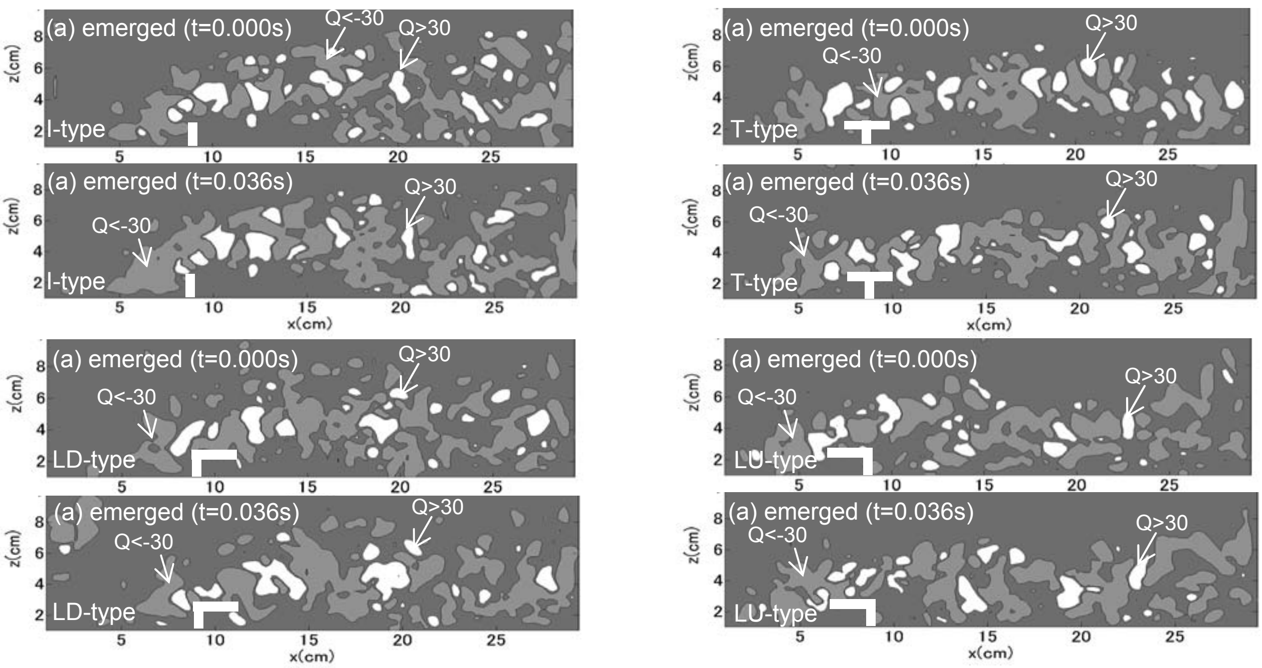

Figure 6(a). Distributions and time variations of Weiss function (Q-value) [1/s] under emerged condition

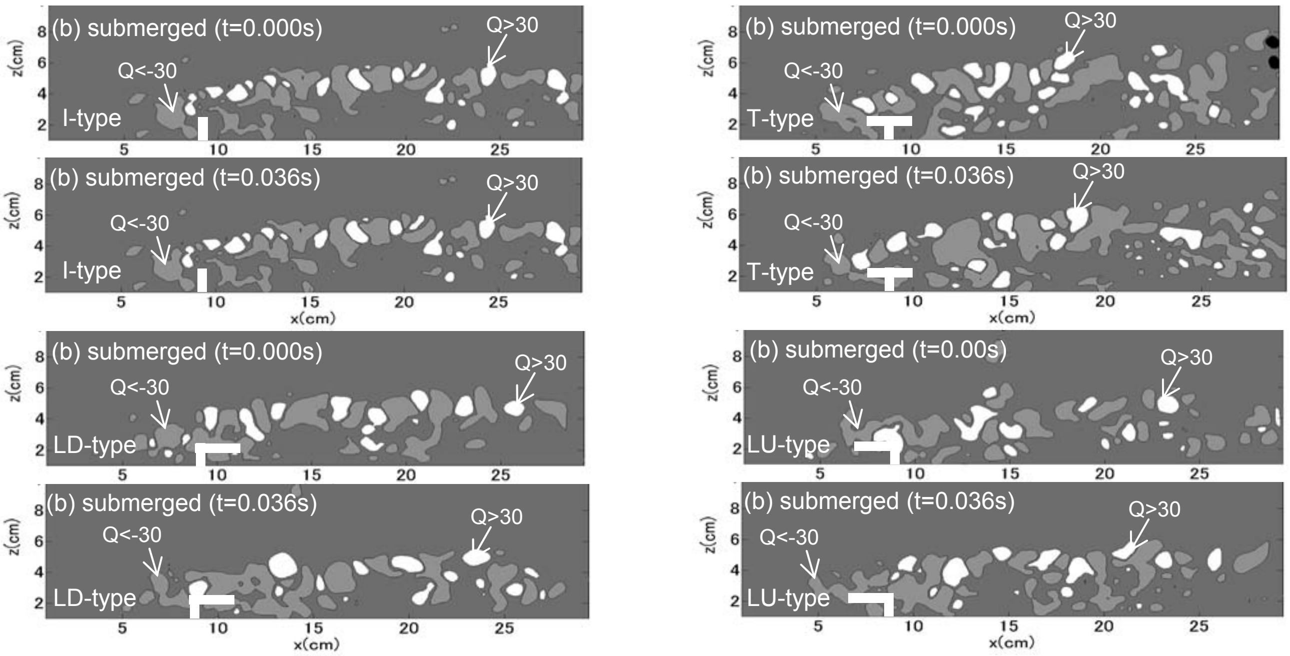

Figure 6(b). Distributions and time variations of Weiss function (Q-value) [1/s] under submerged condition

6(a), the shear force and rotation are distributed alternatively from the tip of the groyne to the downstream end. In the case of groynes running upstream (T-type and LU-type), the distributions cluster on the right side of the channel. The Reynolds stress in Figure 4 also has a similar profile and is distributed near the right side.

The Q-value under submerged conditions is distributed similarly and alternately as shown in Figure 6(b). However, the distribution has a smaller scale of shear force and rotation comparing with the distribution under the emerged conditions, and the distribution clusters in the main stream. The velocity difference between the main stream and dead zone decreases because of the effect of submerged flow on the top surface of the groyne. Therefore, the shear force and rotation decrease. This tendency is significant in the vicinity of the groyne tip.

The areas of shear force and rotation generated from the groyne tip to the downstream show the time variation of stream-wise advection. In the case of groynes running upstream (T-type and LU-type) under emerged conditions, the advection is relatively large whereas it is smaller under submerged conditions owing to a small velocity difference. It is considered that the tracing of these areas with time enables estimation of the generation frequency of shear and rotation motion quantitatively.

As an alternative method to analyze the coherent motions, conditional sampling analysis is applied. For the purpose of strict conditional sampling, the detection function and threshold value have to be defined carefully. The detection function in Equation (1) is defined as

$$I(x,z,t) \equiv \begin{cases} 1: u < 0, w > 0 \;\&\; |uw/u'w'| \geq H \\ 0: otherwise \end{cases} \quad (3)$$

where u' and w' are the root-mean-square values for u and w fluctuations respectively. H is the threshold value, which is estimated from the distribution of the power spectrum density and the typical frequency of instantaneous velocity signals at the fixed point of Equation (1), as shown in Figure 7. The fixed point (x, z) is defined very close to the tips of several types of groynes. The directions of u and w in Equation (1) are defined to select the ejection-like motion developed from the fixed point in this study. The coherent flow structure as a magnitude of velocity (q) is reasonably sampled by means of the detection function (3) and Equation (1).

Figures 8(a) and 8(b) show the conditionally sampled space–time correlations of the velocity magnitude under emerged and submerged condi-

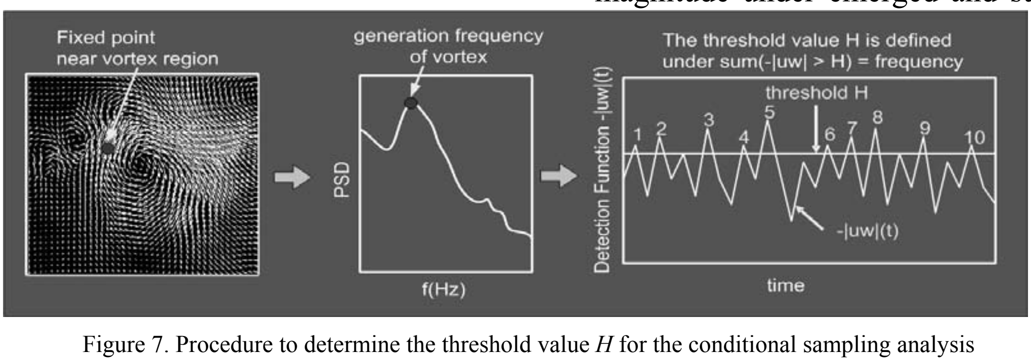

Figure 7. Procedure to determine the threshold value H for the conditional sampling analysis

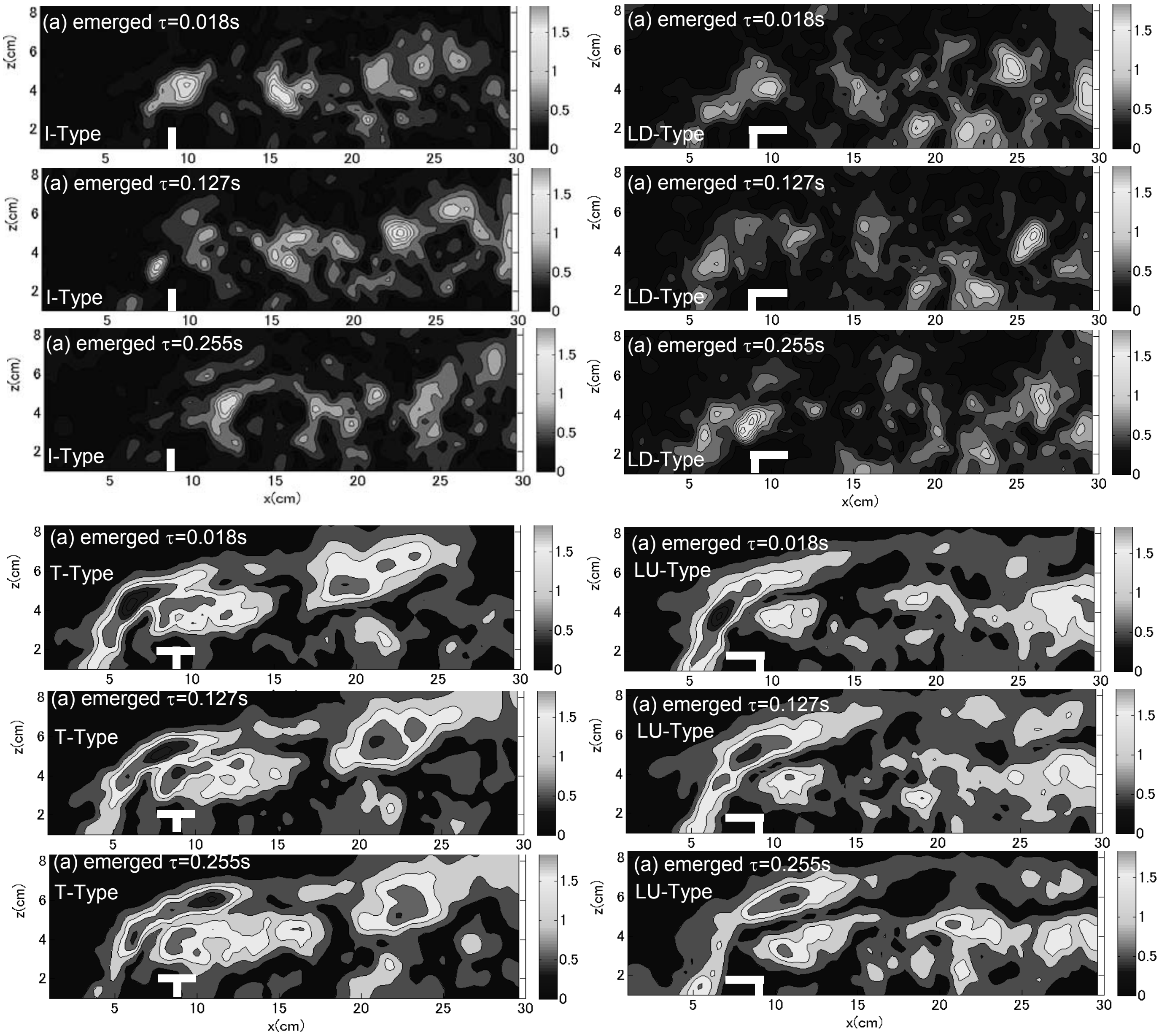

Figure 8(a). Conditionally sampled space-time correlations of velocity magnitude under emerged condition

tions respectively. The sequence of figures indicates the evolution of velocity magnitude since lag time $\tau = 0$ s and at each fixed point.

In the case of groynes running upstream (T-type and LU-type) under emerged conditions, the momentum transport and the sampled velocity magnitude are larger than in other cases, as shown in Figure 8(a). However, a large velocity magnitude is seen around the edge and downstream of the LD-type groyne under submerged conditions, as shown in Figure 8(b). It is considered that these opposing phenomena are related to the vicinity of the vertical flow structure to the groyne. It is supposed that submerged flow over the surface of a groyne generates a vertical downward flow and then a different coherent structure is generated downstream.

The coherent pattern of large velocity magnitude is also seen around tip of LU-type groyne under submerged condition. This pattern is related with velocity difference in plane areas of dead zone and main stream. It is considered that different structure occurs with different types of groyne and submergence.

As for time variations of these coherent patterns, large advection is seen downstream side of emerged groyne heading upstream (T-type and LU-type). The coherent patterns distribute whole area of channel and show similar distribution to the distribution of Reynolds stress of Figure 4. In submerged condition, large coherent pattern is seen near groyne tip and far downstream area of T-type groyne whereas the large pattern is seen only in downstream area of LU-type and LD-type groynes. It can be considered that these coherent flow structures are associated with three dimensional structures and related with shear force around the different shaped groyne.

5 CONCLUSION

The present study focuses on the effects of groyne shapes on the instantaneous-coherent flow and mean flow structures around I-type, T-type,

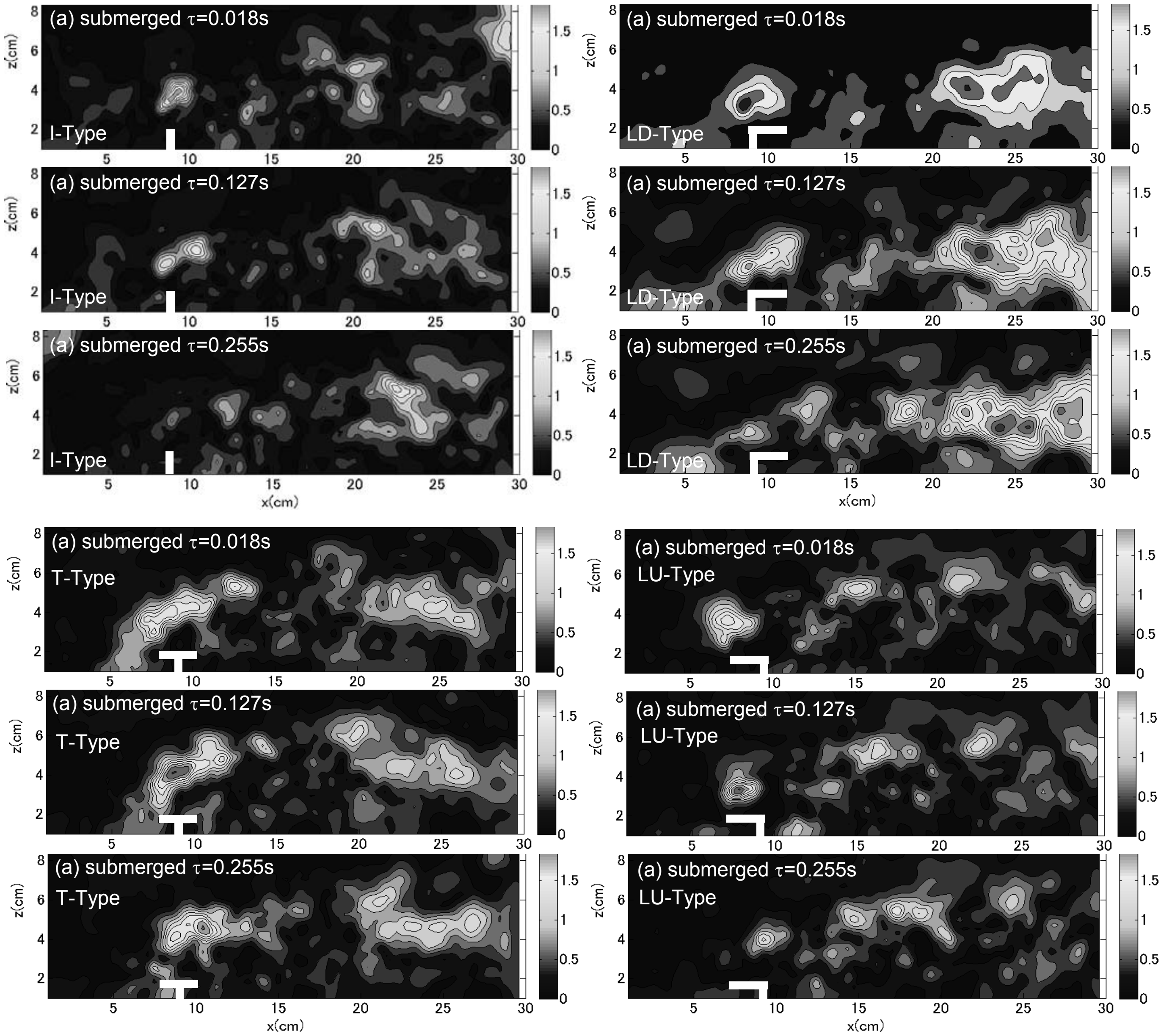

Figure 8(b). Conditionally sampled space-time correlations of velocity magnitude under submerged condition

and L-type groynes. Experiments were conducted with three types of groyne model, using flow visualization and PTV to analyze the resulting images. The experiments investigated a wide area in detail because large-scale vortices are generated downstream of the groynes. Conditional sampling analysis and the Weiss function were applied to reveal the coherent structures and their advection.

The experimental results show the distribution of a large shear layer. Coherent patterns change greatly with the groyne type especially for, L-type groyne. The largely distributed coherent structures are related with formation of sand waves downstream the groyne. To control the bed morphology, these results will be applicable.

REFERENCES

Altai, W. and Chu V.H. 1997. Retention time in a recirculating flow, Proc. XXVI IAHR congress, San Francisco, 9-14.

Chen, F-Y and Ikeda, S. 1997. Horizontal separation flows in shallow open channels with spur dikes, J. Hydroscience and Hydr. Eng. JSCE 15(2), 15-30.

Garde, R.J., Subramanya, K. and Namburdripad, K.D. 1961. Study of scour around spur dikes, J. Hydr. Div. ASCE 87(HY6), 23-37.

Kadota, A., Suzuki, K. and Rummel, A.C. 2007. Shallow flow visualization around a single groyne, Proc. of 7th International Symposium of Particle Image Velocimetry (CD-ROM).

Kuhnle, R.A., Alonso, C.V., Shields, F.D. 2002. Local scour associated with angled spur dikes, J Hydr. Engrg ASCE 128(12), 1087-1093.

Uijttewaal, W.S.J, Lehmann, D. and Mazijk, A. van 2001. Exchange process between a river and its groyne fields: model experiments, J. Hydr. Eng. ASCE, 127(11), 928-936.

Weitbrecht, V. and Jirka, G.H.J. 2001. Flow patterns and exchange processes in dead zones of rivers, Proc. 29th IAHR congress, Beijing, China, theme B, pp.439-445.

Weitbrecht,V. 2004. Influence of Dead-Water Zones on the Dispersive Mass T ransport in Rivers, Doctoral Thesis at University of Karlsruhe.